Flinders UNIVERSITY

Suzuki, D., Kato, H., Ohkawa, M., Anzai, K., Tanaka, H., Limao-Vieira, P., Campbell, L. and Brunger, M.J., 2011. Electron excitation of the Schumann–Runge continuum, longest band, and second band electronic states in O2. Journal of Chemical Physics, 134, 064311.

DOI: http://dx.doi.org/10.1063/1.3533442

Electron excitation of the Schumann–Runge continuum, longest band, and second band electronic states in O2

Daisuke Suzuki, Hidetoshi Kato, Mizuha Ohkawa, Kazutoshi Anzai, Hiroshi Tanaka et al.

Citation: J. Chem. Phys. **134**, 064311 (2011); doi: 10.1063/1.3533442
View online: http://dx.doi.org/10.1063/1.3533442
View Table of Contents: http://jcp.aip.org/resource/1/JCPSA6/v134/i6
Published by the American Institute of Physics.

Electron excitation of the Schumann–Runge continuum, longest band, and second band electronic states in O_2

Daisuke Suzuki,[1] Hidetoshi Kato,[1] Mizuha Ohkawa,[1] Kazutoshi Anzai,[1] Hiroshi Tanaka,[1] Paulo Limão-Vieira,[2] Laurence Campbell,[3] and Michael J. Brunger[3,a)]

[1]*Department of Physics, Sophia University, Chiyoda-ku, Tokyo 102-8554, Japan*
[2]*Laboratório de Colisões Atómicas e Moleculares, Departamento de Física, CEFITEC, Universidade Nova de Lisboa, P-2829-516 Caparica, Portugal*
[3]*ARC Centre for Antimatter-Matter Studies, School of Chemical and Physical Sciences, Flinders University, GPO Box 2100, Adelaide, South Australia 5001, Australia*

(Received 1 November 2010; accepted 13 December 2010; published online 10 February 2011)

We report measurements of differential and integral cross sections for electron excitation of the Schumann–Runge continuum, longest band, and second band electronic states in molecular oxygen. The energy range of the present study is 15–200 eV, with the angular range of the differential cross section (DCS) measurements from 2 to 130°. A generalized oscillator strength analysis is then employed in order to derive integral cross sections (ICSs) from the corresponding DCSs, and these ICSs are compared with relevant energy and oscillator strength scaled Born cross section (BE*f*-scaling [Y.-K. Kim, J. Chem. Phys. 126, 064305 (2007)]) results determined as a part of this investigation. Interestingly, while the present Schumann–Runge continuum and second band ICSs were in reasonable agreement with the respective BE*f*-scaling results, agreement for the longest band was poor below 100 eV with a possible reason for this apparently anomalous behavior being canvassed here. Finally, where possible all present data are compared with the results from earlier measurements and calculations with the level of agreement found being very good in some cases and marginal in others.
 [doi:10.1063/1.3533442]

I. INTRODUCTION

Through the observation of Schumann–Runge (SR) and Tanaka's progression I band systems, as well as its cascade contributions to the populations of its lowest three excited electronic states, it is well known that O_2 plays a vital role in many atmospheric processes. While there have been extensive studies, both measurement and modeling, into the behavior of atoms, molecules, and ions under auroral conditions,[1] only a small subset of these have been devoted to the role of O_2 (Ref. 1). Of these studies, a smaller fraction has concentrated on the effect of electron-driven processes in the electronic-vibrational behavior of O_2 under auroral conditions.[2,3] At least part of the reason for this apparent neglect is that accurate and reliable values for the integral cross sections (ICSs) for the respective relevant excitation processes, over a reasonable electron energy range, have simply not been available. Thus one of the rationales for the present investigation is to provide such data for the important SR continuum, longest band (LB), and second band (SB) transitions.

Another emerging field where cross sections such as these have an important role, if we are to fundamentally understand their behavior, is the realm of low-temperature atmospheric pressure microplasmas.[4] Research in this area includes using microplasmas for material processing, displays, radiation sources, microsatellite propellers, and environmental sensing.[5,6] More recently, they have been shown to have biomedical applications in terms of sterilization, blood coagulation, treatment of ulcers, and fighting against cancer.[4,7] Yet, despite these impressive technological advances, the physics of low-temperature high-pressure discharges is still not fully understood. For instance, in a biomedical application, what is it about these microplasmas that make them so useful in wound treatment? One school of thought suggests that it is the production of $O_2(^1\Delta_g)$, NO, O_3, and OH in the plasmas that give them their useful therapeutic properties. However, without detailed kinetic modeling[8] such an explanation cannot be considered definitive at this time. Such kinetic models, as just one of their inputs, need precisely the type of O_2 cross sections that we present in this paper.

From a more fundamental perspective, it is well known that the SR continuum, LB, and SB states in O_2 all suffer from the effects of extensive Rydberg–valence interactions in varying degrees.[9] In particular, it is generally considered[10–12] that these Rydberg–valence perturbations lead to an anomalous (non-Franck–Condon) behavior in the vibrational intensity distribution of the $E\ ^3\Sigma_u^-$ state. This point is also considered further here. Note that the SR continuum transition refers to the $X\ ^3\Sigma_g^-(v''=0) \rightarrow B\ ^3\Sigma_u^-$ electronic-state excitation, the LB transition refers to the $X\ ^3\Sigma_g^-(v''=0) \rightarrow E\ ^3\Sigma_u^-(v'=0)$ electronic-state excitation and the SB transition refers to the $X\ ^3\Sigma_g^-(v''=0) \rightarrow E\ ^3\Sigma_u^-(v'=1)$ electronic-state excitation. Hence the LB and SB transitions actually arise as excitations from the ground molecular state of O_2 to the lowest two members of the vibrational progression in the excited $E\ ^3\Sigma_u^-$ electronic state. In addition, we have previously found for a number of molecules, including H_2O (Ref. 13), CO (Refs. 14 and 15), CO_2 (Ref. 16), H_2 (Ref. 17), and N_2O (Ref. 18),

a)Electronic mail: michael.brunger@flinders.edu.au.

that application of the energy and oscillator strength scaled Born cross section (BE*f*-scaling[19]) approach, for calculating ICSs for dipole-allowed electronic-state transitions, can lead to a very accurate description of the various scattering processes[20] from threshold to 5000 eV. Exceptions to this general statement have only been found in those cases where resonance effects due to the temporary capture of the incident electron by the target and contamination from an accidentally degenerate or near-degenerate triplet state have arisen. Note this latter statement implicitly assumes a singlet ground electronic-state which was usually the case in the molecules we have previously studied.[13–18] In this study we, therefore, also explore the efficacy of the BE*f*-scaling approach in providing accurate ICSs for the SR, LB, and SB states in O_2, which might be used in atmospheric and technological modeling investigations. Note that as the ground electronic-state of O_2 is a triplet state, the dipole-allowed transitions we probe here are those of a triplet to triplet nature.

Previous differential cross section (DCS) experiments in the SR continuum include those from Wakiya,[21] Johnson and Kanik,[22] Shyn *et al.*,[23] Trajmar *et al.*[24] and Xu *et al.*[25] Some of these data were also used to determine corresponding ICSs. In addition, ICSs for this excitation process have been reported by Lassettre *et al.*,[26] Newell *et al.*,[27], and from an electron-swarm analysis by Hake and Phelps.[28] Impact parameter ICS calculations due to Laricchiuta *et al.*[29] and Garrett *et al.*,[30] as well as a Born–Ochkur level computation from Chung and Lin[31] and a BE*f*-scaling result from Xu *et al.*, for excitation of the SR continuum are also available in the literature. With respect to the LB and SB transitions, the situation in terms of existing data is even more limited. For these states we only know of experimental DCS results from Johnson and Kanik, Trajmar *et al.*, Xu *et al.*, and Shyn *et al.*[32] We note that no theoretical DCS results currently appear to exist for excitation of both the LB and SB transitions, as well as for the SR continuum. With regard to the ICSs, we only have experimental results from Trajmar *et al.*, Newell *et al.*, and Shyn *et al.*[32] and a BE*f*-scaling theoretical result from Xu *et al.* As we shall see later, agreement between these various data and the data and theory, for each of the SR, LB, and SB excitation processes, is often quite marginal. Hence another rationale for this study is to try and resolve these discrepancies and also extend the energy range of the available data.

In Sec. II of this paper we describe our measurement and analysis techniques and procedures. Thereafter, a brief outline of the BE*f*-scaling theory is provided. In Sec. IV we provide results and a discussion, followed by some conclusions from the present study.

II. EXPERIMENTAL DETAILS AND ANALYSIS TECHNIQUES

The present spectrometer[33] consists of an electron gun with a hemispherical monochromator, a molecular beam crossed at right angles to the incident electrons, and a rotatable detector ($\theta = -10^\circ$ to 130°) with a second hemispherical analyzer system. A number of electron optic elements image and energy control the electron beam, with their performance having been checked by detailed electron trajectory calculations. Both the monochromator and analyzer are housed in differentially pumped boxes, in order to reduce the effect of any background gases and to minimize the stray electron background. The target molecular beam is produced by effusing O_2 through a simple nozzle with an internal diameter of 0.3 mm and a length of 5 mm.

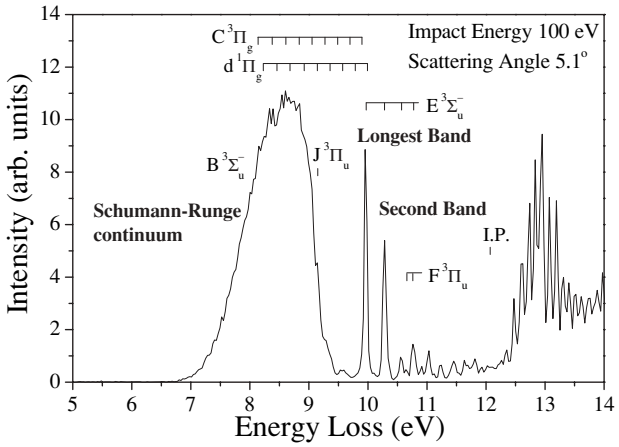

FIG. 1. Typical energy loss spectrum for electron impact excitation of the relevant electronic states in O_2, at an impact energy of 100 eV and at a scattering angle of 5.1°.

The incident electron energies (E_0) of the present study were 15, 20, 30, 50, 100, and 200 eV, and the scattered electron angle (θ) range was $\sim 2^\circ$ to 130°. In all of these cases the energy resolution was in the range of 40−60 meV [full width at half maximum (FWHM)] and the angular resolution was $\sim \pm 1.5^\circ$ (FWHM). The primary electron beam current was typically in the range of 3−15 nA. The incident electron energy was calibrated with respect to the 19.37 eV resonance of He (Ref. 34).

Electron energy loss spectroscopy (EELS) spectra were measured, at each incident electron energy and each scattered electron angle, over the energy-loss range encompassing the elastic peak and from 4.9 eV to 14.4 eV. A typical example of these data at $E_0 = 100$ eV and $\theta = 5.1^\circ$ is shown in Fig. 1, where we note that the elastic peak has been omitted for the sake of clarity. The absolute scales were set using the relative flow technique[35] with helium elastic DCSs as the standard.[36] Note that for each of the SR continuum, LB, and SB that this approach sets their respective manifold DCSs, for the incident electron energy and electron scattering angle in question. For the incident energies of interest ($E_0 = 15$–200 eV) and the energy-loss range of interest ($\Delta E \cong 0$–10.4 eV), the ratio of the energy loss to the incident energy varies roughly in the range of $0 \leq \Delta E/E_0 \lesssim 0.69$. Thus it is crucial to establish the transmission of the analyzer over this energy-loss range, with our procedure for doing so being found in Kato *et al.*[15] We also note the approach of Allan[37] in this regard.

Experimental errors on the present DCSs are estimated at about 18%−25%, including components due to the uncertainty in our analyzer transmission response, an uncertainty due to errors associated with the elastic normalization cross sections, uncertainties due to any fluctuations in target

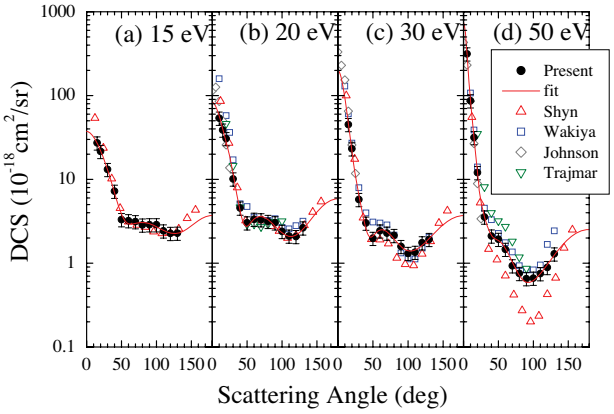

FIG. 2. Differential cross sections (10^{-18} cm^2/sr) for electron impact excitation of the SR continuum in O_2 at the incident electron energies (a) 15 eV, (b) 20 eV, (c) 30 eV, and (d) 50 eV. Present data are compared to the earlier results of Shyn *et al.*,[23] Wakiya,[21] Johnson and Kanik,[22] and Trajmar *et al.*[24] (see legend on figure for further details). The fits to the present data using Eqs. (3)–(5) are also shown at each energy. Note that the highest energy data from Trajmar *et al.* was actually measured at 45 eV.

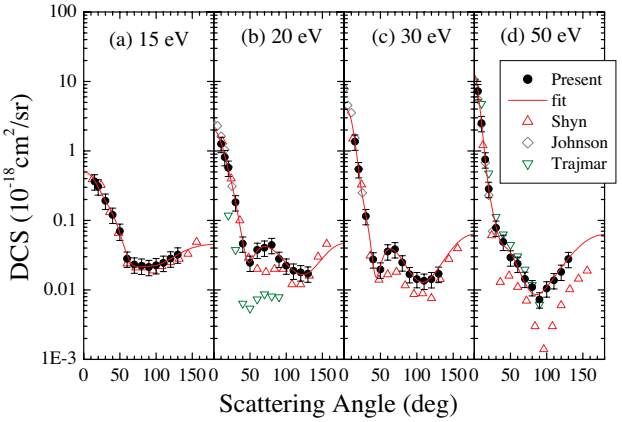

FIG. 4. Differential cross sections (10^{-18} cm^2/sr) for electron impact excitation of the SB in O_2 at the incident electron energies (a) 15 eV, (b) 20 eV, (c) 30 eV, and (d) 50 eV. Present data are compared to the earlier results of Shyn *et al.*,[32] Johnson and Kanik,[22] and Trajmar *et al.*[24] (see legend on figure for further details). The fits to the present data using Eqs. (3)–(5) are also shown at each energy. Note that the highest energy data from Trajmar *et al.* was actually measured at 45 eV.

density and/or the incident electron beam current during the measurements. The present 15, 20, 30, and 50 eV experimental DCSs for the SR continuum, LB, and SB are plotted in Figs. 2–4 and tabulated in Tables I–III with a full discussion of them being given later in Sec. IV of this paper.

The so-determined values of θ and DCS(θ), for each electronic state, are then transformed to K^2 and G_{expt} using the standard formula[38]

$$G_{\text{expt}}(K^2) = \frac{(E/R)k_i a_0}{4a_0^2 k_f a_0} K^2 \text{DCS}(E_0, \theta), \qquad (1)$$

where k_i and k_f are the initial and final momenta of the incident electron, a_0 is the Bohr radius (0.529 Å), R is the Rydberg energy (13.6 eV), E is the excitation energy for each electronic state, $G_{\text{expt}}(K^2)$ is the experimental generalized

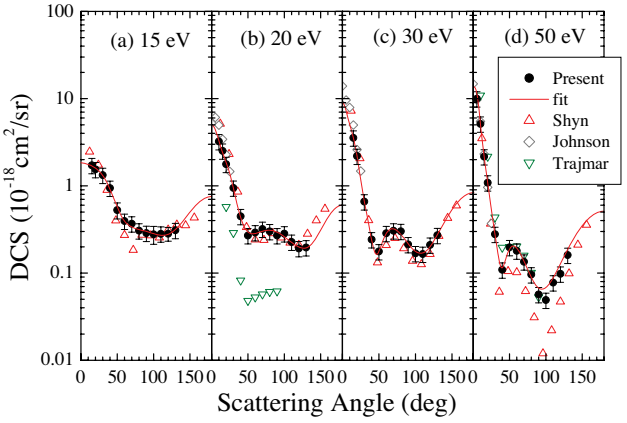

FIG. 3. Differential cross sections (10^{-18} cm^2/sr) for electron impact excitation of the LB in O_2 at the incident electron energies (a) 15 eV, (b) 20 eV, (c) 30 eV, and (d) 50 eV. Present data are compared to the earlier results of Shyn *et al.*,[30] Johnson and Kanik,[22] and Trajmar *et al.*[24] (see legend on figure for further details). The fits to the present data using Eqs. (3)–(5) are also shown at each energy. Note that the highest energy data from Trajmar *et al.* was actually measured at 45 eV.

TABLE I. Electron impact excitation DCSs ($\times 10^{-18}$ cm^2/sr) for the Schumann–Runge continuum in O_2. The estimated uncertainty in the DCS data is typically 18%.

Scattering angle	Impact energy (eV)					
(degrees)	15	20	30	50	100	200
2.14						981.0
3.1					804.5	
3.14						522.0
4.1					551.7	
4.14						308.7
5.0				314.6		
5.1					388.6	
5.14						181.8
6.1					269.1	
7.14						83.01
8.1					136.1	
9.14						37.00
10		53.82		86.80		
10.1					70.15	
14.14						5.205
15	27.26	38.80	45.14	31.57		
15.1					17.04	
20	21.57	30.69	23.17	12.06		
30	13.14	10.13	5.757	3.561		
40	7.234	4.556	3.010	2.113		
50	3.313	3.033	1.980	1.928		
60	3.217	3.346	2.432	1.465		
70	3.133	3.299	2.287	0.931		
80	2.858	3.153	2.143	0.755		
90	2.879	3.036	1.584	0.654		
100	2.879	2.397	1.310	0.663		
110	2.430	2.108	1.350	0.751		
120	2.269	2.081	1.753	0.889		
130	2.281	2.639	1.922	1.291		

TABLE II. Electron impact excitation DCSs ($\times 10^{-19}$ cm^2/sr) for the longest band in O_2. The estimated uncertainty in the DCS data is typically 19%.

Scattering angle	Impact energy (eV)					
(degrees)	15	20	30	50	100	200
2.14						383.2
3.1					273.8	
3.14						223.0
4.1					216.1	
4.14						135.0
5.0				99.82		
5.1					160.3	
5.14						103.8
6.1					126.4	
7.14						60.27
8.1					77.70	
9.14						35.38
10		32.27		51.38		
10.1					46.96	
14.14						5.799
15	17.19	25.19	35.55	21.65		
15.1					17.00	
20	15.45	17.71	21.94	10.87		
30	13.28	9.472	6.598	2.791		
40	9.430	4.470	2.425	1.091		
50	5.275	2.696	1.768	1.972		
60	3.949	2.918	2.860	1.798		
70	3.680	3.198	3.062	1.349		
80	3.065	3.004	3.016	0.961		
90	2.870	2.699	2.131	0.569		
100	2.780	2.833	1.681	0.491		
110	2.819	2.272	1.652	0.777		
120	2.826	1.917	2.101	0.980		
130	3.096	1.963	2.714	1.608		

oscillator strength (GOS), and K^2 is the momentum transfer squared defined by

$$K^2 = (k_i a_0)^2 + (k_f a_0)^2 - 2(k_i a_0)(k_f a_0)\cos\theta. \tag{2}$$

Vriens[39] proposed the following formula to represent the GOS for a dipole-allowed excitation, based on the analytic properties as identified by Lassettre[40] and Rau and Fano:[41]

$$G(x) = \frac{1}{(1+x)^6}\left[\sum_{m=0}^{\infty}\frac{f_m x^m}{(1+x)^m}\right], \tag{3}$$

where

$$x = \frac{K^2}{\alpha^2}, \tag{4}$$

$$\alpha = \sqrt{B/R} + \sqrt{(B-E)/R}. \tag{5}$$

Here B is the binding energy of the target electron being excited. In Eq. (3) the f_m are fitting constants to be determined in a least-squares fit analysis of the experimental GOSs. The results from this analysis, for each electronic state and each incident electron energy, after being converted back into DCS, are shown in Figs. 2–4. Clearly from these figures we see that the fits to the data are very good, a necessary prerequisite in order to derive accurate values for the corresponding ICSs.

Finally, estimates of the ICS at each energy can be obtained from Eqs. (3) to (5) using the standard formulas[42]

$$\mathrm{ICS}(E_0) = \frac{4\pi a_0^2}{E_0/R}\int_{K^2_{\min}}^{K^2_{\max}}\frac{G(K^2)}{E/R}d\ln(K^2), \tag{6}$$

with

$$K^2_{\min} = 2\frac{E_0}{R}\left[1 - \frac{E}{2E_0} - \sqrt{1-\frac{E}{E_0}}\right], \tag{7}$$

$$K^2_{\max} = 2\frac{E_0}{R}\left[1 - \frac{E}{2E_0} + \sqrt{1-\frac{E}{E_0}}\right]. \tag{8}$$

The results for each electronic state, from this latter process, are listed in Table IV and plotted in Figs. 5–7. They are discussed in more detail in Sec. IV.

TABLE III. Electron impact excitation DCSs ($\times 10^{-19}$ cm^2/sr) for the second band in O_2. The estimated uncertainty in the DCS data is typically 25%.

Scattering angle	Impact energy (eV)					
(degrees)	15	20	30	50	100	200
2.14						265.5
3.1					196.8	
3.14						150.0
4.1					134.8	
4.14						91.31
5.0				72.38		
5.1					88.59	
5.14						50.98
6.1					65.17	
7.14						19.09
8.1					33.28	
9.14						8.954
10		12.62		25.13		
10.1					20.59	
14.14						0.833
15	3.640	8.156	13.59	7.541		
15.1					4.046	
20	3.077	5.713	5.458	2.835		
30	1.919	1.821	1.152	0.782		
40	1.203	0.463	0.274	0.491		
50	0.700	0.246	0.196	0.293		
60	0.281	0.377	0.357	0.237		
70	0.232	0.405	0.384	0.144		
80	0.222	0.442	0.248	0.109		
90	0.213	0.279	0.168	0.073		
100	0.226	0.223	0.143	0.105		
110	0.245	0.189	0.135	0.138		
120	0.283	0.179	0.143	0.182		
130	0.323	0.171	0.170	0.278		

TABLE IV. Present ICSs (10^{-18} cm^2) for the Schumann-Runge continuum, longest band, and second band in O_2. The estimated uncertainty in the ICS data are 25%, 25%, and 30%, respectively.

Impact energy (eV)	Integral cross section					
	BE*f* (SR)	Present (SR)	BE*f* (LB)	Present (LB)	BE*f* (SB)	Present (SB)
8.44	0.000					
9.5	21.46					
9.97	25.40		0.000			
10.28	27.57		1.056		0.000	
10.5	28.96		1.348		0.131	
11	31.72		1.792		0.243	
11.5	34.07		2.092		0.323	
12	36.10		2.314		0.390	
13	39.42		2.623		0.502	
14	42.00		2.828		0.593	
15	44.04	57.37	2.971	6.243	0.670	0.728
16	45.68		3.072		0.736	
17	47.00		3.146		0.793	
18	48.06		3.198		0.842	
19	48.92		3.236		0.885	
20	49.60	64.23	3.261	5.180	0.922	0.926
25	51.28		3.282		1.048	
30	51.31	56.81	3.215	5.545	1.111	1.123
35	50.55		3.115		1.139	
40	49.42		3.004		1.146	
45	48.11		2.892		1.141	
50	46.73	50.08	2.782	3.646	1.129	1.133
60	43.98		2.579		1.092	
70	41.41		2.399		1.050	
80	39.07		2.242		1.006	
90	36.96		2.103		0.964	
100	35.05	38.48	1.981	1.917	0.924	0.925
200	23.31	23.30	1.266	1.191	0.649	0.600
300	17.70		0.943		0.504	
400	14.39		0.758		0.415	
500	12.18		0.636		0.355	
600	10.61		0.550		0.311	
700	9.413		0.485		0.277	
800	8.479		0.435		0.251	
900	7.725		0.395		0.229	
1000	7.103		0.362		0.212	
2000	4.035		0.202		0.122	
3000	2.874		0.142		0.088	
4000	2.253		0.111		0.069	
5000	1.862		0.091		0.057	

III. BE*f*-SCALING DETAILS

A full description of the BE*f*-scaling approach that we have employed here, to calculate ICSs for the SR continuum, LB, and SB, can be found in Kim.[38] Hence only a brief discussion of the more important details need to be given here. Note that the scaled (plane-wave) Born cross sections that we used in conjunction with this technique are not only subject to the approximations in the collision theory part, but also depend on the accuracy of the wave functions used for the initial and final states of the target molecule.

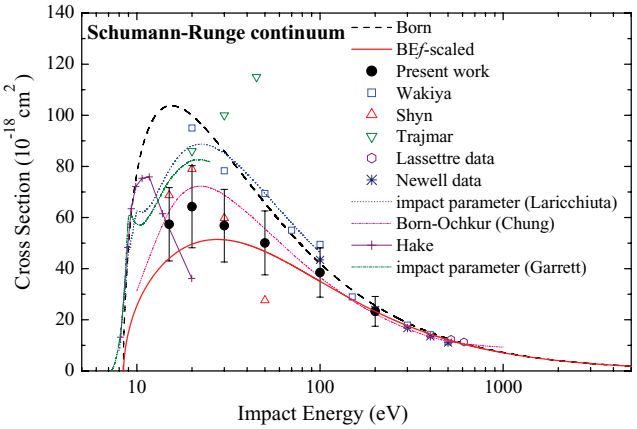

FIG. 5. Integral cross sections (10^{-18} cm^2) for electron impact excitation of the SR continuum in O_2. See legend on the figure for further details.

The *f*-scaled Born cross sections (ICS_f) are given by[38]

$$ICS_f(E_0) = \frac{f_{accur}}{f_{Born}} ICS_{Born}(E_0), \tag{9}$$

where f_{accur} is an accurate optical oscillator strength (OOS) value from either accurate target wave functions or experiments and f_{Born} is the OOS from the same wave functions used to calculate the unscaled Born cross sections $ICS_{Born}(E_0)$. The *f*-scaling process has the effect of replacing the wave functions used for ICS_{Born} with accurate wave functions. We note that the $ICS_{Born}$for the SR continuum were calculated from the experimental GOS of Xu *et al.*,[25] and accurate OOS were used from the work of Chan *et al.*[43] On the other hand, the ICS_{Born} for the LB, and SB were calculated from the theoretical work of Li *et al.*,[10] while the required accurate OOSs were used from Ogawa and Ogawa[44] and Lewis *et al.*,[45] respectively.

In addition the BE-scaled Born cross sections (ICS_{BE}) are given by

$$ICS_{BE}(E_0) = \frac{E_0}{(E_0 + B + E)} ICS_{Born}(E_0). \tag{10}$$

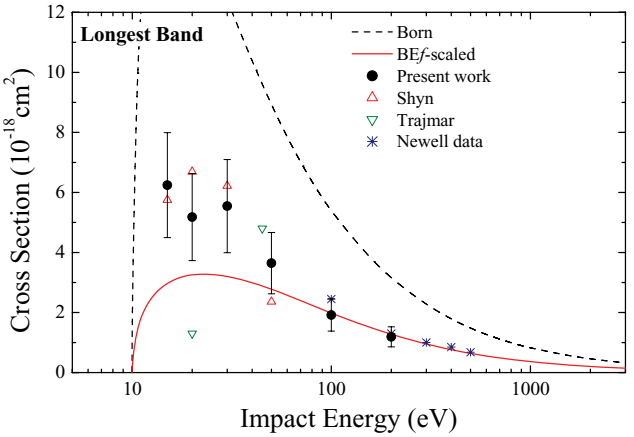

FIG. 6. Integral cross sections (10^{-18} cm^2) for electron impact excitation of the LB in O_2. See legend on the figure for further details.

This scaling corrects the well known deficiency of the Born approximation at low E_0without losing its established validity at high E_0 (Ref. 38).

If an unscaled $\mathrm{ICS_{BE}}(E_0)$ is obtained from poor or marginal wave functions while an accurate OOS is known, then both *f*-scaling and BE-scaling can be applied to obtain a BE*f*-scaled Born cross section [$\mathrm{ICS_{BE}}_f(E_0)$]:

$$\mathrm{ICS_{BE}}_f(E_0) = \frac{f_{\mathrm{accur}}}{f_{\mathrm{Born}}} \frac{E_0}{E_0 + B + E} \mathrm{ICS_{Born}}(E_0). \qquad (11)$$

The current calculated $\mathrm{ICS_{BE}}_f(E_0)$ are listed for the SR continuum, LB, and SB in Table IV. While we note that Xu *et al.* have also reported BE*f*-scaling results for the LB and SB, which are consistent with the present, the current $\mathrm{ICS_{BE}}_f(E_0)$ are given on a much finer energy grid than provided by Xu *et al.* The present BE*f*-scaling results for the SR continuum have not been previously reported. A detailed comparison between our BE*f*-scaling results, for each transition, and the corresponding ICS measurements is given in Sec. IV. A comparison of both the present theory and measured ICSs with previous data and computations is also given in Sec. IV.

IV. RESULTS AND DISCUSSION

In Tables I–III, we respectively present our electron scattering differential cross sections for excitation of the SR continuum, LB, and SB states in O_2. A selection of those data, along with the results from some previous studies,[21–24,32] for incident electron energies in the range of 15–50 eV are also respectively given in Figs. 2–4. Note that in all these plots the present error bars are at the one standard deviation level. Before considering each of these figures in more detail, there are some general trends which we can collectively note from them. Firstly, all the present DCSs are forward peaked in magnitude as you go to smaller scattered electron angles, with this degree of forward peak increasing as the incident electron energy increases. This result is consistent with all the previous[21–24,32] experimental investigations. As molecular oxygen is a homonuclear diatomic with no permanent dipole moment, we believe these observations are consistent with the important role that the long-range polarization potential must be playing in the scattering dynamics[46]

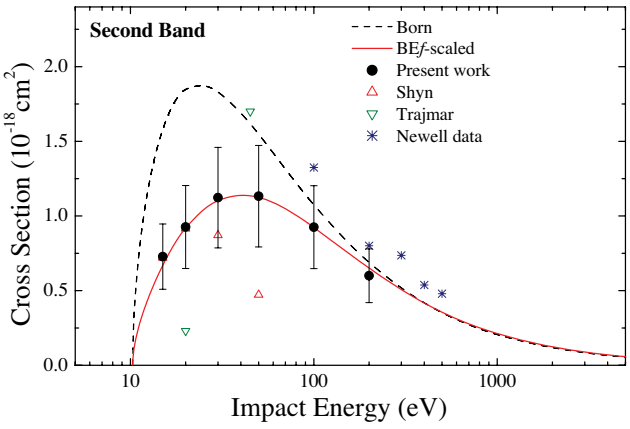

FIG. 7. Integral cross sections (10^{-18} cm^2) for electron impact excitation of the SB in O_2. See legend on the figure for further details.

of these processes. In support of this we also note the relatively large value of the dipole polarizability [$\alpha = 1.5812 \times 10^{-24}$ cm^3 (Ref. 47)] that O_2 possesses, confirming the rather diffuse nature of the electron density of the target. Secondly, at 20 and 30 eV (see Figs. 2–4) all three states have structures in their angular distributions, that is, reminiscent of the decay of a *d*-wave shape resonance into each state. However, there is no supporting evidence for this explanation in any of the ICS plots (see Figs. 5–7). As a consequence, we believe that this oscillatory structure, at middle angles in the SR continuum, LB, and SB angular distributions, is more likely to be due to constructive/destructive interference effects between the dominant partial waves describing their scattering dynamics. Finally, it is clear from Figs. 2–4 that under some kinematic conditions some of the previous measurements agree well with those of the present, but under other kinematic conditions agreement between the earlier and present DCSs is rather marginal. Notwithstanding this observation, we now believe that a body of DCS data for the SR continuum, LB, and SB states exists against which theoretical calculations, such as from the R-matrix theory,[48] could be benchmarked. Note that in viewing Figs. 2–4 recall that the *y*-axis scales are over a four or five decade log-scale.

Considering Fig. 2 in more detail we find that at 15, 20, and 30 eV, the present SR continuum DCSs and those of Shyn *et al.*[23] are in quite good accord, except at the most forward and more backward scattered electron angles. This observation is probably not too surprising as it has been well documented,[46] particularly in the elastic channel, that data from the group of Shyn and colleagues often overestimates the magnitude of DCSs at small and large scattering angles. At 50 eV, however, for scattering angles $> 25^\circ$, the agreement between the present DCS and Shyn *et al.* is very poor, with Shyn *et al.* significantly underestimating the magnitude of the SR continuum DCS. This is a somewhat surprising result, as any instrumental energy-dependent analyzer transmission effect would be expected to be more significant at energies closer to threshold. Although a comparison with the data of Johnson and Kanik[22] can only be made over a more limited energy and angular range, agreement between our measurements and their results is generally very good. A reasonable level of accord is also typically found between us and the SR continuum DCS of Wakiya, at 20, 30, and 50 eV. Finally, we note that when we compare our work with that of Trajmar *et al.*, we see satisfactory agreement at 20 eV, in terms of the shape and magnitude of the DCS, but only a marginal level of agreement at 50 eV. A similar story to that just described above for the SR continuum is also found for the LB (see Fig. 3) and SB (see Fig. 4) states. The only exceptions to this general statement are that there are now no data from Wakiya to compare against, the 45 eV DCS data of Trajmar *et al.* for both the LB and SB is now in good agreement with the present while the 20 eV DCS data of Trajmar *et al.*, again for both the LB and SB transitions, are in very poor agreement (see Figs. 3 and 4) with our data, particularly in regard to the magnitude of these DCSs. In this latter case, the most likely reason for this discrepancy is an analyzer transmission problem with their spectrometer[24] in measuring DCS for the $E\,^3\Sigma_u^-(v' = 0, 1)$ states.

Using the techniques described in Sec. II, the above DCSs were extrapolated to 0° and 180° (see Figs. 2–4 for the results of these fits) and then integrated to determine the corresponding ICSs. Tabulated values of those ICSs are given in Table IV for the SR continuum, the LB and also for the SB. Also provided in Table IV are the relevant BE*f*-scaling results (see Sec. III) for each of those states. In Fig. 5 we now compare our theoretical and experimental ICS results for the SR continuum against the earlier crossed-beam data of Wakiya, Shyn *et al.*[23], Trajmar *et al.*, Lassettre *et al.*, and Newell *et al.* and results from a swarm-based analysis from Hake and Phelps.[28] Also plotted are some impact parameter theoretical results from Laricchiuta *et al.*[29] and Garrett *et al.*[30] and a Born–Ochkur level computation from Chung and Lin.[31] It is clear from Fig. 5 that the trend in our 15–200 eV SR-continuum ICSs is in very good agreement with the higher energy data of Lassettre *et al.* and Newell *et al.* The present ICS data is also largely consistent, within our stated uncertainties, with the Born–Ochkur calculation of Chung and Lin and our own BE*f*-scaling computation. Both the impact parameter calculations[29,30] are, at 15 eV and 20 eV, higher in magnitude than the present measurements, even when we allow for the errors on those experimental ICSs. In addition, they both predict a near-threshold structure in the SR-continuum ICS. As these types of calculations are quite simplistic, we are skeptical as to whether that feature is in fact physical. Note that the work of Garrett *et al.* and Laricchiuta *et al.* predict incorrect thresholds for the SR continuum, suggesting some problems with their target description of the SR continuum. With regard to the level of accord between the present ICSs and some of the other lower (<100 eV) energy measurements, we find that the observed trend is consistent with what we found earlier in our discussion of the DCSs. Namely, at some energies the present data is in good agreement with that from Shyn *et al.*[23] or Wakiya, but at others this agreement is more marginal. Agreement with the measurements of Trajmar *et al.*, on the other hand, except at 20 eV where it is fair, is quite poor. While the absolute values of our experimental SR-continuum ICSs are somewhat systematically higher in magnitude (see Fig. 5) than our corresponding BE*f*-scaling results for energies less than about 100 eV, they are still consistent with one another. Nonetheless, as indicated in Fig. 1, there are at least two further electronic states of O_2 that overlap with the $B\,^3\Sigma_u^-$ state of the SR continuum. These states could well be making a contribution to our measured flux (cross section) in the energy-loss range of interest, which would explain why our measured ICSs are somewhat higher in magnitude than the BE*f*-scaling result in Fig. 6 which is for the $B\,^3\Sigma_u^-$ state only. As a consequence, we recommend that the present SR continuum BE*f*-scaling results would be appropriate cross sections to incorporate in any atmospheric[3] or air plasma[4] modeling studies.

The first significant feature we notice in Fig. 6, ICSs for the electron impact excitation of the LB, is that there is significantly less measured data and no other theory against which we can compare the present results. For this excitation process we see, within their respective uncertainties, the results of Shyn *et al.*[32] are largely consistent with the present work and both sets are typically, for energies less then 50 eV, much stronger in magnitude than the current BE*f*-scaling calculation. While for energies greater than 50 eV our BE*f*-scaling result is in very good agreement with the present experimental ICSs and those of Newell *et al.*, this discrepancy at lower energies precludes the use of our BE*f*-scaling results for the LB in any modeling studies. Rather an interpolation and extrapolation (to threshold) process using the measured ICSs would be needed here to determine a valid set for modeling purposes. We believe that the origin of this breakdown, in the applicability of the BE*f*-scaling method, is due to the well known[12] strong Rydberg-valence perturbations that affect the $E\,^3\Sigma_u^-(v'=0)$ state in O_2. In addition, we also believe that this could be a general limitation in the BE*f*-scaling approach. Namely that any vibrational sublevel of an electronic state in any molecule, where avoided level crossings and other perturbation effects are important, might not have their cross sections reliably calculated within the BE*f*-scaling approach. This stands in total contrast to our previous experience in CO (Ref. 14), where the BE*f*-scaling ICS results for all of the $A\,^1\Pi(v'=0-8)$ vibrational sublevels were in excellent agreement with the measured data.

Finally, in Fig. 7, we examine our results for the SB. In this case agreement at the lower energies with the results from Trajmar *et al.* is quite poor, while agreement (or at least the trend in agreement) at the higher energies with Newell *et al.* is also now quite marginal (unlike what we found for both the SR continuum and the LB). For energies less than 30 eV, the present SB integral cross sections and those from Shyn *et al.*[32] are in fair agreement. Perhaps the most stunning aspect of Fig. 7 is the remarkable level of agreement between the present measured cross sections and those calculated using the BE*f*-scaling approach. Hence, contrary to what we just concluded for the LB transition, in the case of the SB excitation our BE*f*-scaling results will be totally appropriate for use in any modeling studies in which O_2 is an important constituent. This is an interesting observation as it suggests that the SB transition, compared to that for the LB state, is relatively unperturbed by the Rydberg-valence interactions. This is in spite of them being separated by only ~0.32 eV (see Fig. 1). However, such an observation is entirely consistent with the results in Lewis *et al.*[12] and so we believe it is valid. We again highlight the lack of any available *ab initio* theoretical results, for this and the other states, against which we can compare our results.

V. CONCLUSIONS

We have reported new measurements of differential and integral cross sections for the electron impact excitation of the SR continuum, LB, and SB in molecular oxygen. Agreement between the present data and the earlier available measurements was "patchy," and strongly depended on the kinematical conditions being considered. Nonetheless, we now believe there is in totality a body of reliable cross section data against which *ab initio* level theories might test their various formalisms. We have also reported BE*f*-scaling ICS results for each of these transitions, which for the SR continuum and SB were found to be in good agreement with our measurements. This led us to conclude that these BE*f*-scaling re-

sults will be very useful for scientists attempting to model the behavior of phenomena (e.g., atmospheric pressure plasmas and the Earth's atmosphere) in which O_2 plays a role. Unfortunately, our BE*f*-scaling results for excitation of the LB severely underestimated the magnitude of the experimental cross sections, at energies less than ~50 eV, and so cannot be employed in such modeling studies. This failure of the BE*f*-scaling approach, in this case, we believe is due to the strong Rydberg-valence interactions which significantly perturb the $E\ ^3\Sigma_u^-(v'=0)$ state in O_2. We note that the present BE*f*-scaling results for both the LB and SB are consistent with the values reported by Xu *et al.*[25] in an earlier study.

The ICSs we have determined in this investigation are rather different from those employed by Jones *et al.*,[3] in their original study of the electronic-vibrational role played by O_2 in our atmosphere. As a consequence we foreshadow here a new study into the role of electron-driven processes in the electronic-vibrational behavior of O_2 in our atmosphere, in which the present O_2 ICS are incorporated. Such a study will also, compared to the results in Jones *et al.*[3], enable us to investigate the sensitivity of atmospheric macroscopic behavior (e.g., atmospheric radiative emissions) to the underlying microscopic (e.g., cross sections) inputs.

Finally, we have noticed previously[13,14,16] that the BE*f*-scaling method is effective with respect to describing single channels for optically allowed transitions. This was the case of the $A\ ^1\Pi$ state in CO, which is well isolated from the other electronic states in that molecule. However, as indicated for the unresolved (experimentally) overlapping bands for the optically allowed ($C\ ^1\Pi$ and $D\ ^1\Sigma^+$) and optically forbidden ($d\ ^3\Pi$ and $2\ ^3\Pi$, respectively) states in N_2O (Ref. 18), by assuming the BE*f*-scaling ICSs are correct and by using the measured data one might deduce the cross sections for the relevant optically forbidden states. For the optically forbidden case, the ICSs show, in general, a maximum near the excitation threshold which decays rapidly as you go to higher energies. Thus, the deviation of the lower energy experimental ICSs from those of the BE*f*-scaling results should in principle serve to provide the unknown cross sections for the optically forbidden states. This represents a potential new utility for the BE*f*-scaling method that we have not canvassed before.

ACKNOWLEDGMENTS

This work was conducted under the support of the Japanese Ministry of Education, Sport, Culture and Technology. Additional support from the Australian Research Council, through its Centres of Excellence Program, is further noted. One of us (Paulo Limão-Vieira) acknowledges his visiting professor position at Sophia University, Tokyo, Japan. This work forms part of the EU COST Actions CM0601 and CM0805 programmes "ECCL" and "The Chemical Cosmos," respectively. We all thank Professor Y. Itikawa for his fruitful suggestions in regard to these measurements.

[1] D. J. Strickland, J. Bishop, J. S. Evans, T. Majeed, P. M. Shen, R. J. Cox, R. Link, and R. E. Huffman, J. Quant. Spectrosc. Radiat. Transf. **62**, 689 (1999).
[2] D. C. Cartwright, S. Trajmar, and W. Williams, Ann. Geophys. (C.N.R.S) **28**, 397 (1972).
[3] D. B. Jones, L. Campbell, M. J. Bottema, P. J. O. Teubner, D. C. Cartwright, W. R. Newell, and M. J. Brunger, Planet. Space Sci. **54**, 45 (2006).
[4] F. Iza, J. K. Lee, and M. G. Kong, Phys. Rev. Lett. **99**, 075004 (2007).
[5] J. J. Shi and M. G. Kong, Phys. Rev. Lett. **96**, 105009 (2006).
[6] K. H. Becker, K. H. Schoenbach, and J. G. Eden, J. Phys. D **39**, R55 (2006).
[7] G. C. Kim, G. J. Kim, S. R. Park, S. M. Jeon, H. J. Seo, F. Iza, and J. K. Lee, J. Phys. D **42**, 032005 (2009).
[8] M. J. Kushner, J. Appl. Phys. **95**, 846 (2004).
[9] H. Lefebvre-Brion and R. W. Field, *Perturbations in the Spectra of Diatomic Molecules* (Academic, Orlando, 1986).
[10] Y. Li, M. Honigmann, K. Bhanuprakash, G. Hirsch, R. J. Buenker, M. A. Dillon, and M. Kimura, J. Chem. Phys. **96**, 8314 (1992).
[11] M. Kimura, M. A. Dillon, R. J. Buenker, G. Hirsch, Y. Li, and L. Chantranupong, Z. Phys. D: At. Mol. Clusters **38**, 165 (1996).
[12] B. R. Lewis, J. P. England, S. T. Gibson, M. J. Brunger, and M. Allan, Phys. Rev. A **63**, 022707 (2001).
[13] P. A. Thorn, M. J. Brunger, P. J. O. Teubner, N. Diakomichalis, T. Maddern, M. A. Bolorizadeh, W. R. Newell, H. Kato, M. Hoshino, H. Tanaka, H. Cho, and Y.-K. Kim, J. Chem. Phys. **126**, 064306 (2007).
[14] H. Kawahara, H. Kato, M. Hoshino, H. Tanaka, and M. J. Brunger, Phys. Rev. A **77**, 012713 (2008).
[15] H. Kato, H. Kawahara, M. Hoshino, H. Tanaka, M. J. Brunger, and Y.-K. Kim, J. Chem. Phys. **126**, 064307 (2007).
[16] H. Kawahara, H. Kato, M. Hoshino, H. Tanaka, L. Campbell, and M. J. Brunger, J. Phys. B **41**, 085203 (2008).
[17] H. Kato, H. Kawahara, M. Hoshino, H. Tanaka, L. Campbell, and M. J. Brunger, Phys. Rev. A **77**, 062708 (2008).
[18] H. Kawahara, D. Suzuki, H. Kato, M. Hoshino, H. Tanaka, O. Ingólfsson, L. Campbell, and M. J. Brunger, J. Chem. Phys. **131**, 114307 (2009).
[19] Y.-K. Kim, Phys. Rev. A **64**, 032713 (2001).
[20] M. J. Brunger, P. A. Thorn, L. Campbell, H. Kato, H. Kawahara, M. Hoshino, H. Tanaka, and Y.-K. Kim, J. Phys.: Conf. Ser. **115**, 012004 (2008).
[21] K. Wakiya, J. Phys. B **11**, 3913 (1978).
[22] P. V. Johnson and I. Kanik, J. Phys. B **34**, 3041 (2001).
[23] T. W. Shyn, C. J. Sweeney, A. Grafe, and W. E. Sharp, Phys. Rev. A **50**, 4794 (1994).
[24] S. Trajmar, W. Williams, and A. Kuppermann, J. Chem. Phys. **56**, 3759 (1972).
[25] W.-Q. Xu, J.-M. Sun, Y.-Y. Wang, and L.-F. Zhu, Phys. Rev. A **82**, 042716 (2010).
[26] E. N. Lassettre, S. M. Silverman, and M. E. Krasnow, J. Chem. Phys. **40**, 1261 (1964).
[27] W. R. Newell, M. A. Khakoo, and A. C. H. Smith, J. Phys. B **13**, 4877 (1980).
[28] R. D. Hake and A. V. Phelps, Phys. Rev. **158**, 70 (1967).
[29] A. Laricchiuta, R. Celiberto, and M. Capitelli, Chem. Phys. Lett. **329**, 526 (2000).
[30] B. C. Garrett, L. T. Redmon, C. W. McCurdy, and M. J. Redmon, Phys. Rev. A **32**, 3366 (1985).
[31] S. Chung and C. C. Lin, Phys. Rev. A **21**, 1075 (1980).
[32] T. W. Shyn, C. J. Sweeney, and A. Grafe, Phys. Rev. A **49**, 3680 (1994).
[33] H. Tanaka, T. Ishikawa, T. Masai, T. Sagara, L. Boesten, M. Takekawa, Y. Itikawa, and M. Kimura, Phys. Rev. A **57**, 1798 (1998).
[34] J. N.H. Brunt, G. C. King, and F. H. Read, J. Phys. B **10**, 1289 (1977).
[35] S. K. Srivastava, A. Chutjian, and S. Trajmar, J. Chem. Phys. **63**, 2659 (1975).
[36] L. Boesten and H. Tanaka, At. Data Nucl. Data Tables **52**, 25 (1992).
[37] M. Allan, J. Phys. B **38**, 3655 (2005).
[38] Y.-K. Kim, J. Chem. Phys. **126**, 064305 (2007).
[39] L. Vriens, Phys. Rev. **160**, 100 (1967).
[40] E. N. Lassettre, J. Chem. Phys. **43**, 4479 (1965).
[41] A. R.P. Rau and U. Fano, Phys. Rev. **162**, 68 (1967).
[42] B. H. Bransden and C. J. Joachain, *Physics of Atoms and Molecules* (Longmans, London, 1983).
[43] W. F. Chan, G. Cooper, and C. E. Brion, Chem. Phys. **170**, 99 (1993).
[44] S. Ogawa and M. Ogawa, Can. J. Phys. **53**, 1845 (1975).
[45] B. R. Lewis, S. T. Gibson, M. Emami, and J. H. Carver, J. Quant. Spectrosc. Radiat. Transf. **40**, 469 (1988).
[46] M. J. Brunger and S. J. Buckman, Phys. Rep. **357**, 215 (2002).
[47] A. C. Newell and R. C. Baird, J. Appl. Phys. **36**, 3751 (1965).
[48] J. Tennyson, Phys. Rep. **491**, 29 (2010).